JCI insight

HDL activation of endothelial sphingosine-1-phosphate receptor-1 ($S1P_1$) promotes regeneration and suppresses fibrosis in the liver

Bi-Sen Ding, … , Shahin Rafii, Timothy Hla

JCI Insight. 2016;1(21):e87058. https://doi.org/10.1172/jci.insight.87058.

Research Article **Therapeutics** **Vascular biology**

Regeneration of hepatic sinusoidal vasculature is essential for non-fibrotic liver regrowth and restoration of its metabolic capacity. However, little is known about how this specialized vascular niche is regenerated. Here we show that activation of endothelial sphingosine-1-phosphate receptor-1 ($S1P_1$) by its natural ligand bound to HDL (HDL-S1P) induces liver regeneration and curtails fibrosis. In mice lacking HDL-S1P, liver regeneration after partial hepatectomy was impeded and associated with aberrant vascular remodeling, thrombosis and peri-sinusoidal fibrosis. Notably, this “maladaptive repair” phenotype was recapitulated in mice that lack $S1P_1$ in the endothelium. Reciprocally, enhanced plasma levels of HDL-S1P or administration of SEW2871, a pharmacological agonist specific for $S1P_1$ enhanced regeneration of metabolically functional vasculature and alleviated fibrosis in mouse chronic injury and cholestasis models. This study shows that natural and pharmacological ligands modulate endothelial $S1P_1$ to stimulate liver regeneration and inhibit fibrosis, suggesting that activation of this pathway may be a novel therapeutic strategy for liver fibrosis.

JCI insight

RESEARCH ARTICLE

HDL activation of endothelial sphingosine-1-phosphate receptor-1 ($S1P_1$) promotes regeneration and suppresses fibrosis in the liver

Bi-Sen Ding,[1,2] Catherine H. Liu,[3] Yue Sun,[1] Yutian Chen,[1] Steven L. Swendeman,[3,4] Bongnam Jung,[5] Deebly Chavez,[2] Zhongwei Cao,[1,2] Christina Christoffersen,[6,7] Lars Bo Nielsen,[6,7,8] Susan R. Schwab,[9] Shahin Rafii,[2] and Timothy Hla[3,4]

[1]Key Laboratory of Birth Defects and Related Diseases of Women and Children, Ministry of Education, State Key Laboratory of Biotherapy, West China Second University Hospital, Sichuan University, and Collaborative Innovation Center for Biotherapy, Chengdu, China. [2]Ansary Stem Cell Institute, Division of Regenerative Medicine, Department of Medicine, Weill Cornell Medicine, New York, New York, USA. [3]Center for Vascular Biology, Department of Pathology and Laboratory Medicine, Weill Cornell Medicine, Cornell University, New York, New York, USA. [4]Vascular Biology Program, Boston Children's Hospital, Department of Surgery, Harvard Medical School, Boston, Massachusetts, USA. [5]Department of Immunology, Genetics and Pathology, Uppsala University, Uppsala, Sweden. [6]Department of Clinical Biochemistry, Rigshospitalet, Copenhagen, Denmark. [7]Department of Biomedical Sciences, [8]Department of Clinical Medicine, University of Copenhagen, Denmark. [9]Department of Pathology, Skirball Institute, New York University School of Medicine, New York, New York, USA.

Regeneration of hepatic sinusoidal vasculature is essential for non-fibrotic liver regrowth and restoration of its metabolic capacity. However, little is known about how this specialized vascular niche is regenerated. Here we show that activation of endothelial sphingosine-1-phosphate receptor-1 ($S1P_1$) by its natural ligand bound to HDL (HDL-S1P) induces liver regeneration and curtails fibrosis. In mice lacking HDL-S1P, liver regeneration after partial hepatectomy was impeded and associated with aberrant vascular remodeling, thrombosis and peri-sinusoidal fibrosis. Notably, this "maladaptive repair" phenotype was recapitulated in mice that lack $S1P_1$ in the endothelium. Reciprocally, enhanced plasma levels of HDL-S1P or administration of SEW2871, a pharmacological agonist specific for $S1P_1$ enhanced regeneration of metabolically functional vasculature and alleviated fibrosis in mouse chronic injury and cholestasis models. This study shows that natural and pharmacological ligands modulate endothelial $S1P_1$ to stimulate liver regeneration and inhibit fibrosis, suggesting that activation of this pathway may be a novel therapeutic strategy for liver fibrosis.

Introduction

Liver diseases that culminate in cirrhosis pose a major health problem worldwide (1–7). Effective strategies to stimulate liver regeneration may provide a novel therapeutic option. The liver has the capacity to regenerate after damage (8–19), and resection of 70% of liver mass in mammals by partial hepatectomy (PH) induces rapid regrowth of functional liver tissue. Liver regeneration requires complex interactions between replicating hepatocytes and expanding non-parenchymal cells such as stellate cells (1, 2, 18, 20), vascular endothelial cells (ECs) (21–27), and hematopoietic cells (6, 28, 29). Disruption of the hepatocyte-endothelium crosstalk in the injured liver frequently results in impaired regeneration and maladaptive healing (3, 30–35), which is characterized by the formation of scar tissue (fibrosis) (1, 2, 28, 29, 36–38), ultimately leading to the clinical condition of cirrhosis. Therefore, identification of key cellular and molecular mechanisms involved in hepatic regeneration is an important goal in the development of novel strategies to control liver-related diseases (39–41).

The regenerating liver relies on regrowth of functional sinusoidal vascular network that distributes the blood flow between systemic and portal circulation. Dysfunctional hepatic vascular system not

Authorship note: C.H. Liu, Y. Sun, and Y. Chen contributed equally to this work.

Conflict of interest: The authors have declared that no conflict of interest exists.

Submitted: February 12, 2016
Accepted: November 3, 2016
Published: December 22, 2016

Reference information:
JCI Insight. 2016;1(21):e87058.
doi:10.1172/jci.insight.87058.

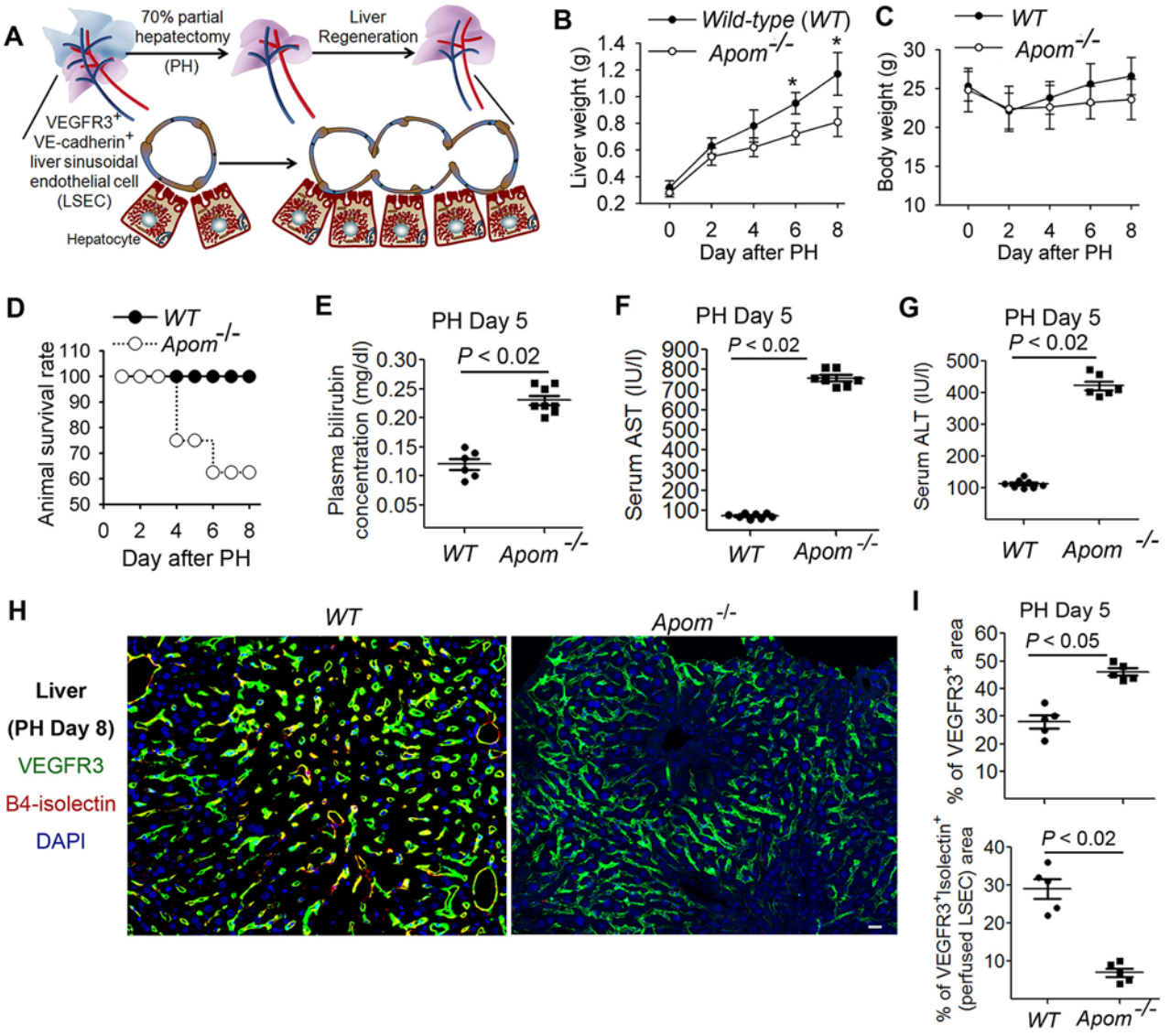

Figure 1. Regeneration of liver mass and vascular structure in mice deficient of HDL component ApoM after partial hepatectomy (PH). (**A**) Strategy to test liver regeneration in mice with genetic depletion of ApoM (*Apom*$^{-/-}$). Both *Apom*$^{-/-}$ and *wild-type* (*WT*) control mice were subjected to surgical resection of 70% liver mass (partial hepatectomy, PH). To perform PH, three most anterior lobes (right medial, left medial and left lateral lobes) (which comprise 70% of the liver weight) were resected without injuring the blood supply to the caudate and the right lobes. Restoration of functional liver mass and vascular architecture after PH was analyzed in both mouse genotypes. Histological analysis of the liver from *WT* and *Apom*$^{-/-}$ mice after sham operation is shown in Supplemental Figure 1A. (**B–G**) Recovery of liver weight (**B**), body weight (**C**), mouse survival rate (**D**), restoration of hepatic function (**E**), and extent of liver parenchymal injury (**F** and **G**) in *Apom*$^{-/-}$ and *WT* mice at indicated time points after PH. Levels of plasma bilirubin and serum aspartate aminotransferase (AST) and alanine aminotransferase (ALT) were measured to examine hepatic function and liver damage. N = 6-8 mice per group. Each dot in the dot plot indicates individual animal throughout all figures. Statistical difference was determined by One way ANOVA throughout Figure 1. (**H** and **I**) Sinusoidal vascular regeneration in hepatectomized mice. Expression of VEGFR3, a specific marker of liver sinusoidal endothelial cell (LSEC) was tested by immunostaining. To examine functional sinusoidal vessels that are perfused, 2 mg/kg B4-Isolectin binding to endothelial cell surface was intravenously (i.v.) injected into the mice after PH. Representative image of immunostaining is shown in **H**, and percentage of VEGFR3$^+$ and isolectin$^+$ vascular area was quantified in (**I**). Note the increased lumen size in non-perfused isolectin$^-$VEGFR3$^+$ liver sinusoidal vasculature of *Apom*$^{-/-}$ mice after PH. N = 5 mice per group. Scale bar = 50 μm.

only suppresses metabolic activity of the liver (42–44) but also induces thrombotic (45, 46) and fibrotic responses (3, 33, 47–50). In particular, hepatic sinusoids are lined with specialized liver sinusoidal endothelial cells (LSECs). As such, functional remodeling of replicated LSEC to connect with the existing vascular system is crucial for liver regeneration. However, how hepatic sinusoidal vascular expansion and remodeling are regulated during liver regeneration and fibrogenesis is not well defined.

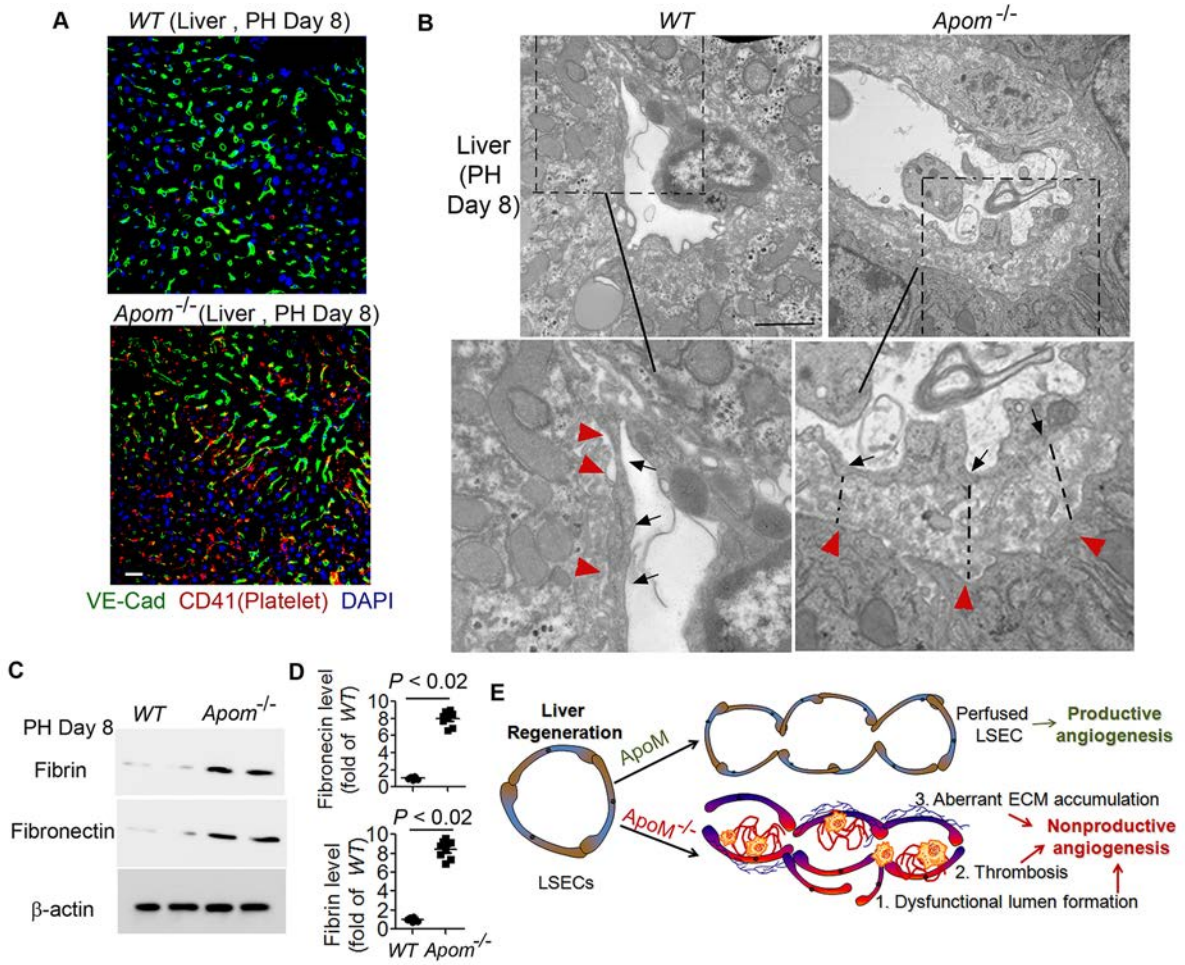

Figure 2. Sinusoidal vascular regeneration is impaired in *Apom*$^{-/-}$ mice, compared to control groups. (**A**) Accumulation of platelets in *WT* and *Apom*$^{-/-}$ groups after PH. Deposited platelets on LSEC was tested by immunostaining of platelet marker CD41 and endothelial VE-Cadherin. Scale bar = 50 μm. Quantification of platelet distribution is shown in Supplemental Figure 2A. (**B**) Ultrastructure of LSEC in *WT* and *Apom*$^{-/-}$ groups after PH was analyzed by transmission electron microscopy. Note that after PH, *Apom*$^{-/-}$ mice exhibited distorted morphology of LSECs, increased LSEC-hepatocyte distance (dashed line), and higher level of perivascular matrix protein (inset). Black arrow and red arrowhead indicate the borders of LSEC and hepatocyte, respectively. Scale bar = 5 μm. (**C** and **D**) Protein levels of fibronectin and fibrin β-chain was examined by immunoblot and quantified by optical density analysis. N = 6-8 mice per group. Statistical difference was determined by One way ANOVA. (**E**) Loss of HDL component ApoM in mice leads to "maladaptive vascular remodeling" in the liver after PH, prohibiting liver regeneration and causing fibrotic injury. This vascular response is characterized by increased peri-sinusoidal deposition of matrix protein, platelet cells, and fibrin clots.

The lipid mediator S1P regulates diverse endothelial functions such as barrier function, vascular maturation and flow signaling (51–58). Plasma S1P is chaperone-bound and signals via S1P receptors to elicit downstream effects. S1P receptor 1 ($S1P_1$) is highly expressed in ECs. HDL-bound S1P acts as a biased agonist of endothelial $S1P_1$, triggering unique signaling response coupled to β-arrestin to inhibit vascular inflammation and pathology (53). This tissue-protective, homeostatic role of HDL-S1P-endothelial $S1P_1$ pathway led us to hypothesize that ligand-dependent modulation of endothelial $S1P_1$ drives regenerative remodeling of LSEC and prevents fibrosis after PH and liver injury.

Results

Deficiency of HDL constituent ApoM in mice (Apom$^{-/-}$*) inhibited liver regeneration after PH.* To test the contribution of HDL-bound S1P in liver regeneration, we first utilized PH model that induces regeneration of residual hepatic lobes without perturbing the integrity of LSEC (Figure 1A) (24). We subjected *Apom*$^{-/-}$ mice, which lack HDL S1P-binding component, Apoliprotein M, and control wild-type (*WT*) mice to PH. Liver tissue from *Apom*$^{-/-}$ mice exhibited similar morphology to control liver after sham operation (Supplemental Figure 1A; supplemental material available online with this article; doi:10.1172/jci.insight.87058DS1). In contrast,

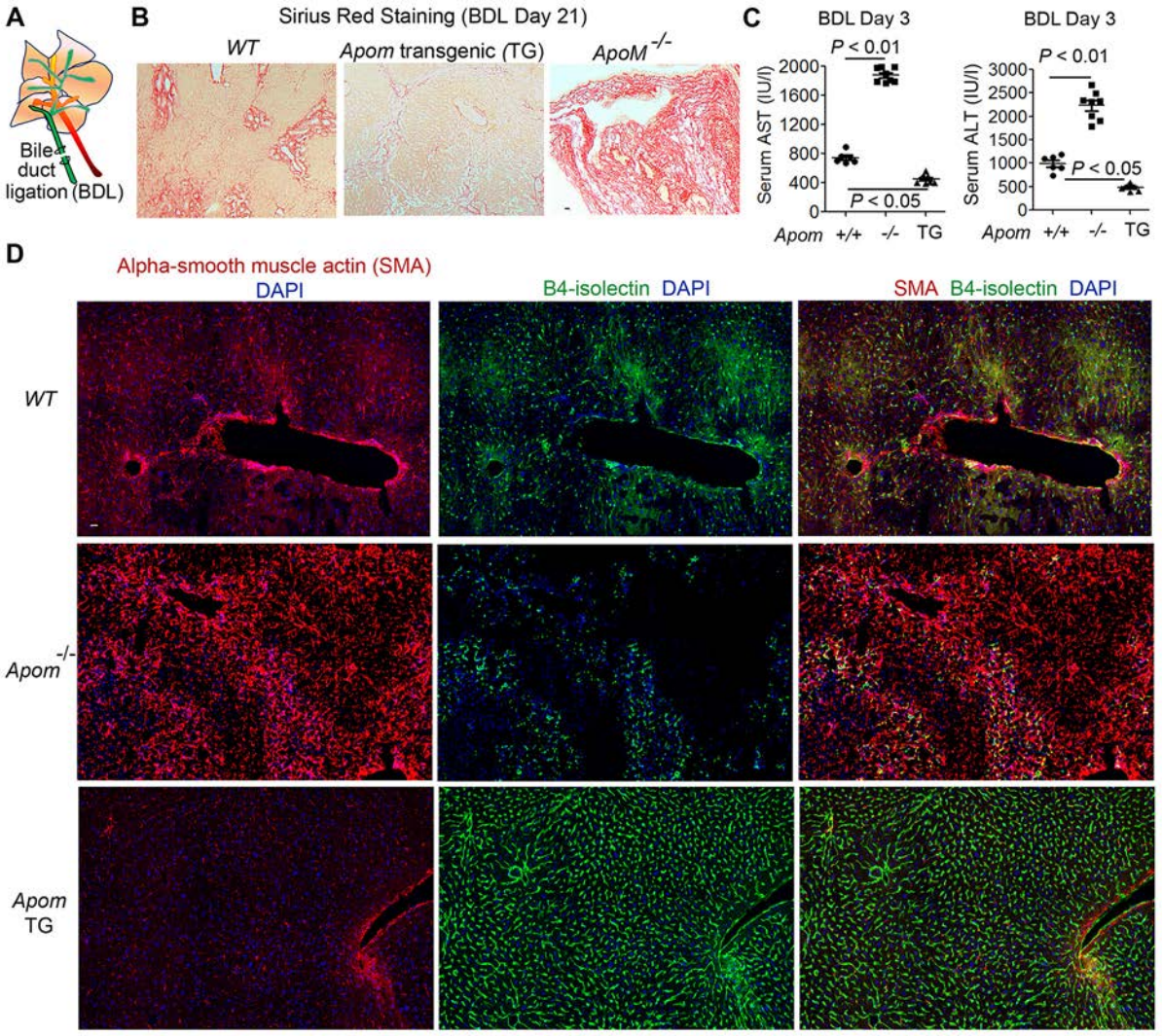

Figure 3. Fibrosis in *Apom* knockout (*Apom*$^{-/-}$) and transgenic mice (*Apom* TG) after bile duct ligation (BDL)-induced biliary epithelial injury. (**A**) Approach to test the influence of ApoM on fibrosis in mouse BDL model. BDL injury was induced by ligating and resecting common bile duct. Fibrosis was analyzed at indicated time points after BDL. (**B** and **C**) After BDL, hepatic damage was assessed in *WT*, *Apom*$^{-/-}$ and *Apom* TG mice overexpressing 10-fold of physiological ApoM level. Sirius red staining (**B**) and serum levels of AST and ALT (**C**) were used examine collagen deposition and liver injury of indicated mouse groups, respectively. Scale bar = 50 μm in Figure 2. N = 6-8 mice per group. Statistical difference was determined by One way ANOVA. (**D**) Tile scan confocal image of stained liver section of *WT*, *Apom*$^{-/-}$ and *Apom* TG mice 21 days after BDL. Fluorescently labeled B4-Isolectin was i.v. injected into mice 5 minutes before sacrificing to label perfused blood vessel. Liver cryosection was stained with antibody recognizing α-smooth muscle actin (SMA). Global distribution of fluorescence in the liver section was analyzed by tile scan confocal microscopy.

regenerative responses after PH were significantly inhibited in *Apom*$^{-/-}$ mice compared to the control group, as evidenced by decreased liver weight, increased animal lethality, and elevated levels of plasma bilirubin and serum Aspartate aminotransferase (AST) and Alanine aminotransferase (ALT) (Figure 1, B–G, and Supplemental Figure 1B). These data suggest that HDL-S1P promotes functional recovery of liver mass after PH.

Impaired new vascular formation in hepatectomized Apom$^{-/-}$ *mice is associated with perivascular fibrosis and thrombosis*. We and others previously showed that one of the key steps of liver regeneration is the replication of LSEC to expand the hepatic sinusoidal vascular network (24, 25). More importantly, nascent LSECs need to assemble into perfused sinusoidal vessels to allow hepatic blood circulation, which requires complex interactions between existing vascular system and surrounding parenchymal and stromal cells. We therefore characterized the nascent LSEC in *Apom*$^{-/-}$ and WT mice after PH.

To measure whether the hepatic vasculature is perfused by blood after PH, 2 mg/kg of *Griffonia simplicifolia* lectin (B4-isolectin) was intravenously (i.v.) injected into hepatectomized mice. Isolectin signal was visualized in liver cryosections after co-staining with LSEC marker VEGFR3 (Figure 1H).

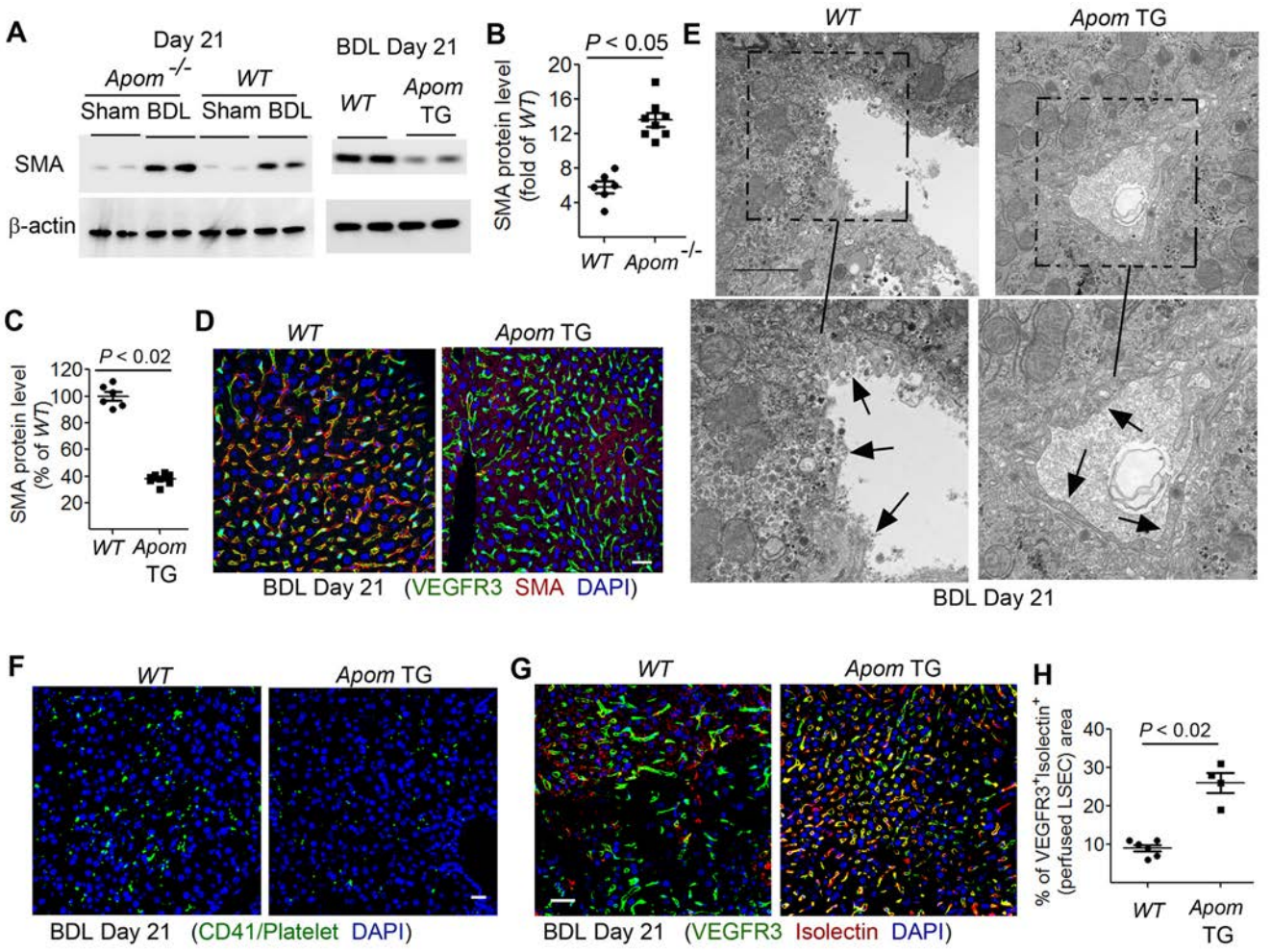

Figure 4. Fibrosis and vascular structure in *WT*, *Apom*$^{-/-}$, and *Apom* TG mouse liver after BDL. (**A–C**) Hepatic SMA protein level in indicated mouse groups was tested by immunoblot. Representative immunoblot image is presented in (**A**), and quantification is shown in (**B**) and (**C**). N = 6-8 mice per group. Statistical difference was determined by One way ANOVA throughout Figure 4. (**D–F**) Peri-sinusoidal accumulation of SMA, vascular ultrastructure, and deposition of platelets after BDL were examined by immunostaining of VEGFR3 and SMA (**D**), transmission electron microscopy (**E**), and CD41 staining (**F**). Arrow in panel E indicates LSEC in the injured liver. Scale bar = 5 μm (**E**), 50 μm (**D** and **F**). Quantification of SMA and platelet deposition in the injured liver are shown in Supplemental Figure 2, B and C. (**G** and **H**) Vascular perfusion in *Apom* TG and control mice after BDL. B4-Isolectin was i.v. injected to identify perfused sinusoidal vessel. Percentage of isolectin$^+$VEGFR3$^+$ vascular area is quantified (**H**). Scale bar = 50 μm; N= 4-6 mice per group.

The emergence of functional LSECs perfused by hepatic blood flow was determined by identifying VEGFR3$^+$ LSECs bound by isolectin (VEGFR3$^+$Isolectin$^+$ LSECs). After PH, the liver of *Apom*$^{-/-}$ mice exhibited morphologically distorted and functionally non-perfused VEGFR3$^+$ sinusoidal vasculature (Figure 1I). Therefore, ApoM contributes to the regeneration of perfused liver vasculature and restoration of functional liver tissue.

The aberrant growth of hepatic sinusoidal vasculature led us to analyze the vascular ultrastructure after PH by transmission electron microscopy (TEM). Compared to control mouse liver exhibiting properly positioned LSECs and hepatocytes, LSEC morphology of *Apom*$^{-/-}$ mice appeared fragmented with enlarged sinusoidal lumen size (Figure 2A). In addition, increased LSEC-hepatocyte distance and perivascular deposition of extracellular matrix (ECM) were observed, suggesting that lack of HDL-bound S1P could cause liver fibrosis. Indeed, immunostaining showed that LSECs of hepatectomized *Apom*$^{-/-}$ mice were closely associated with the ECM protein fibronectin and higher accumulation of platelets and fibrin clots (Figure 2, B–D, and Supplemental Figure 2A). Therefore, *Apom*$^{-/-}$ mice that lack HDL-bound S1P show attenuated hepatic sinusoidal vascular regeneration after PH, leading to a "vascular maladaptive remodeling" phenotype with characteristics of perivascular fibrosis, thrombosis, and formation of nonfunctional dilated sinusoidal vasculature (Figure 2E).

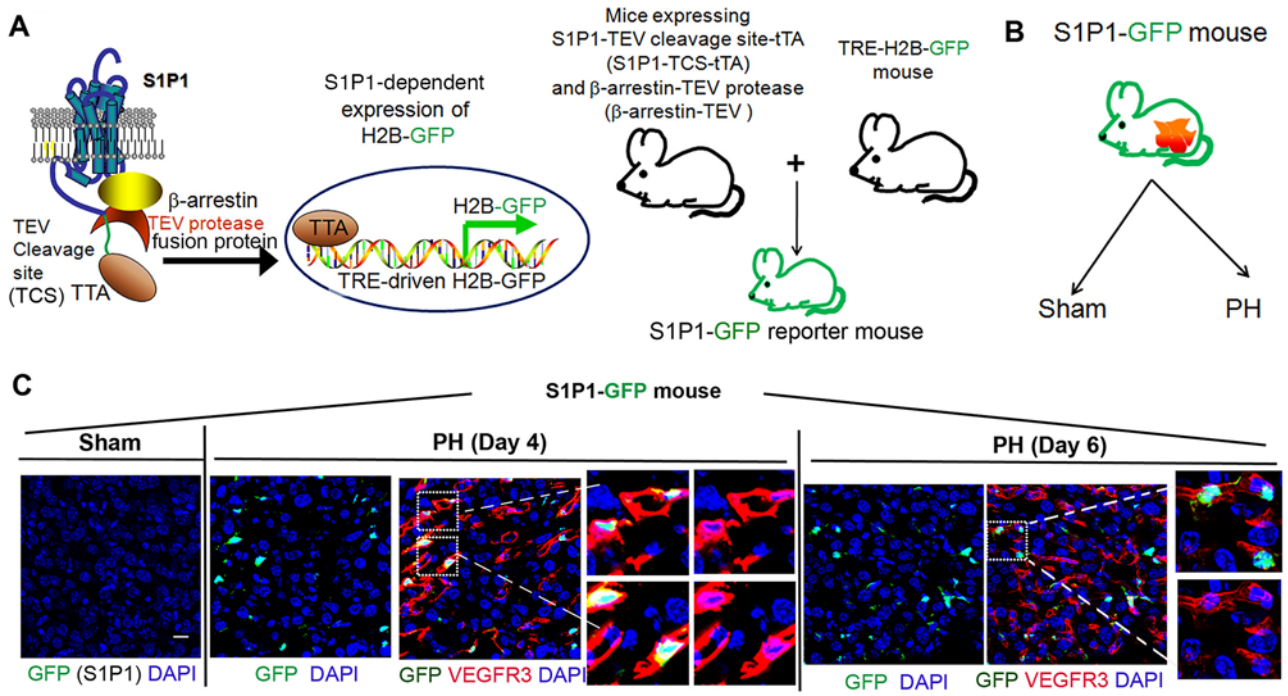

Figure 5. S1P$_1$ signaling in mouse LSEC is involved in vascular regeneration after PH. (**A**) Strategy to generate S1P1-GFP signaling reporter mice. First, because activation of S1P1 recruits arrestins, *S1pr1* gene in mouse is linked to a tetracycline-controlled transactivator (tTA) at its C terminus with a Tobacco Etch Virus (TEV) protease cleavage site (TCS), generating a *S1pr1-TCS-tTA* knockin mouse. Second, a β-arrestin-TEV protease fusion protein was also introduced into *S1pr1-TCS-tTA* mouse. Upon S1P$_1$ activation, this fusion protease is recruited to release tTA from the C terminus of S1P1. Third, in histone H2B-GFP reporter mouse, nuclear entry of released tTA triggers expression of H2B-GFP driven by tetracycline-response element (TRE). (**B**) Schema depicting strategy to test S1P$_1$ activation in the liver following PH. Mouse expressing both *S1p1r-TCS-tTA* and *β-arrestin-TEV* protease were mated with H2B-GFP mice, resulting in S1P$_1$-GFP reporter mouse. Then S1P$_1$-GFP reporter mouse underwent PH and sham procedures. (**C**) After PH, S1P$_1$ signaling (GFP) was mainly localized in VEGFR3$^+$ LSECs, suggesting the role of LSEC S1P$_1$ pathway in modulating liver regeneration. Scale bar = 50 μm.

ApoM exhibits anti-fibrotic function in mice after biliary injury. The phenotype in *Apom*$^{-/-}$ mice after PH suggests an anti-fibrotic role of ApoM and HDL-bound S1P in liver repair. We therefore used the bile duct ligation (BDL), a clinically relevant liver cholestasis model, to define how ApoM affects fibrosis in the injured liver, especially phenotypes accompanying aberrant LSEC remodeling (Figure 3A). Common bile duct was ligated and resected to cause biliary epithelial damage. There was significant collagen deposition, enhanced serum levels of AST and ALT, and upregulation of α-smooth muscle actin (SMA) in the control mouse liver after BDL, as measured by Sirius red staining, SMA immunostaining and immunoblot (Figure 3, B–D, and Figure 4, A–D). Notably, hepatic expression of collagen and SMA protein were markedly upregulated in *Apom*$^{-/-}$ mice but drastically lower in *Apom* transgenic mice (*Apom* TG) and control liver (Supplemental Figure 2B). As such, circulating ApoM reduces fibrogenic response during BDL-induced cholestatic injury.

We then set out to analyze hepatic vascular ultrastructure by TEM in *WT* and *Apom* TG mice after BDL. In *WT* mice, hepatic sinusoidal structure was perturbed by BDL, with a disruption of LSEC layer and compromised cellular structure (Figure 4E). This morphological change was alleviated in *Apom* TG mice. There was also markedly lower extent of platelet deposition and fibrin clot accumulation in *Apom* TG liver than that of control mice (Figure 4F, and Supplemental Figure 2C). In fact, sinusoidal vascular perfusion was improved in *Apom* TG mice, with ameliorated hepatic damage compared to control group (Figure 4, G and H). Therefore, higher level of HDL-bound S1P which is carried by ApoM, prevents "vascular maladaptive remodelling", alleviating fibrosis after liver cholestatic damage.

Activation of ApoM-S1P$_1$ pathway in LSEC is essential for endothelial regeneration without causing fibrosis. The influence of ApoM on sinusoidal vascular phenotype implicates that ApoM promotes liver repair via modulating LSEC function. S1P bound to ApoM-containing HDL acts as a biased agonist for endothelial S1P$_1$ signaling (53). Thus, we tested activation of S1P$_1$ signaling in LSEC after PH with a S1P$_1$ signaling reporter mouse (Figure 5, A and B) (59). This reporter mouse measures signaling by endogenous

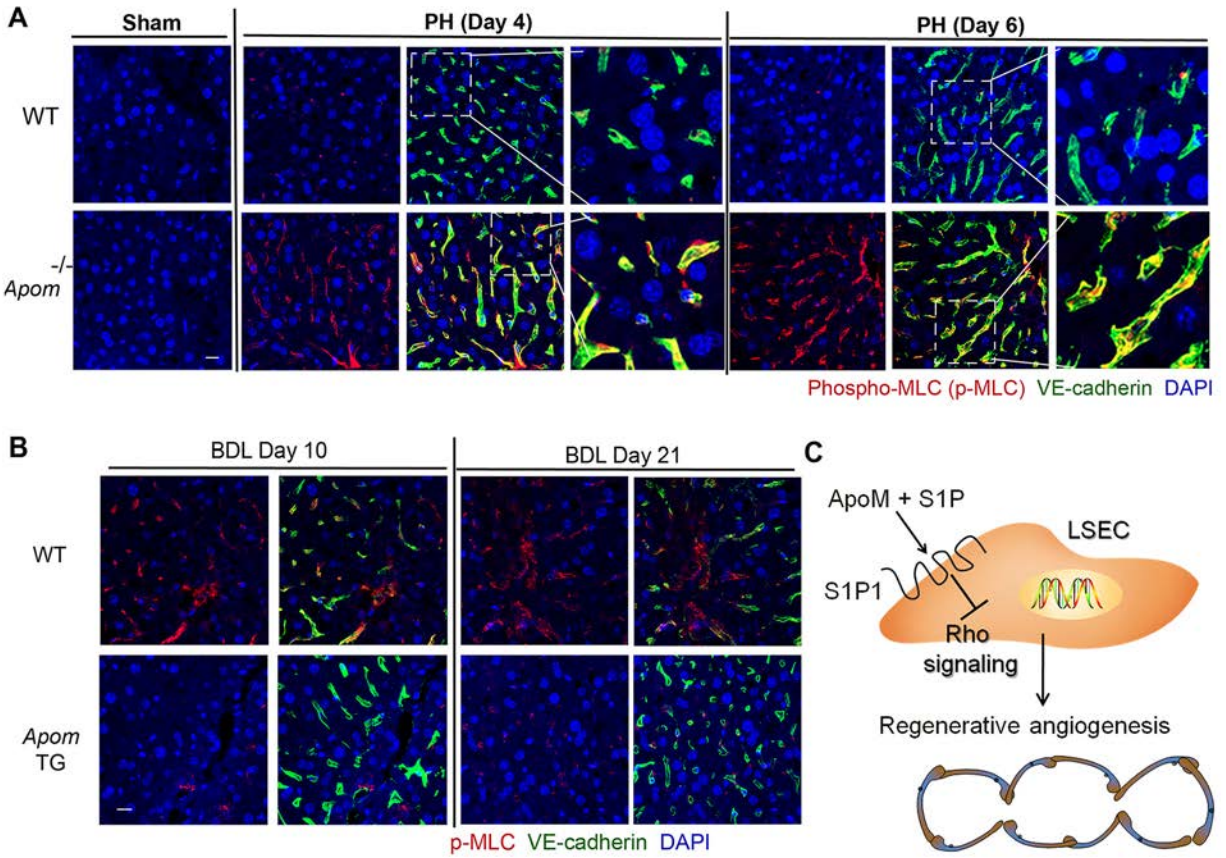

Figure 6. ApoM-S1P$_1$ pathway prevents Rho activation in mouse LSEC after PH and BDL injury. (**A** and **B**) Activation of Rho pathway in LSEC after PH (**A**) and BDL (**B**) was determined by co-staining of phosphorylated myosin light chain (p-MLC) and VE-cadherin. Loss of ApoM (*Apom*$^{-/-}$) causes Rho activation in LSEC after PH, and overexpressing ApoM (*Apom* TG) decreases endothelial Rho activity in BDL-injured liver (B); Scale bar = 50 μm. (**C**) ApoM-endothelial S1P$_1$ pathway prevents activation of Rho signaling in LSEC during liver repair.

S1P$_1$ – a readout that integrates S1P$_1$ expression and ligand availability. In this system, genomic S1P$_1$ is replaced with S1P$_1$ linked at the C terminus to the tetracycline-controlled transactivator (tTA). The linkage possesses a Tobacco Etch Virus (TEV) protease cleavage site, and the mice also express a β-arrestin/TEV protease fusion protein. Activated S1P$_1$ recruits the β-arrestin/TEV protease fusion, which releases the tTA, and in turn stimulates expression of a stable histone 2B (H2B)-GFP. Using this S1P$_1$ signaling reporter, we uncovered that PH preferentially stimulated S1P$_1$ (GFP) signaling in VEGFR3$^+$ LSECs (Figure 5C). implicating the possible contribution of endothelial S1P$_1$ signaling in hepatic and LSEC regeneration following PH.

Since S1P$_1$ activation strongly induces the small GTPase Rac, which is antagonistic to the stimuli that activate the Rho GTPase (60, 61), we studied the involvement of Rho pathway in ApoM-endothelial S1P$_1$ signaling in LSECs. Phosphorylation of myosin light chain (p-MLC), a key downstream target of endothelial Rho pathway activation (62) was tested in VE-cadherin$^+$ LSEC after both PH and BDL. Compared to control mice, *Apom*$^{-/-}$ mice showed markedly enhanced level of p-MLC in LSEC at day 4 and 6 after PH (Figure 6A). Reciprocally, p-MLC level in LSEC of *Apom TG* mice was substantially lower than control animals following BDL injury (Figure 6B). These data suggest that HDL-bound S1P activation of endothelial cell suppresses the Rho pathway, driving pro-regenerative endothelial remodelling and bypassing fibrotic and thrombotic injuries (Figure 6C).

Mice with endothelial cell-specific S1P$_1$ deficiency (S1pr1$^{i\Delta EC/i\Delta EC}$) recapitulates phenotype of Apom$^{-/-}$ mice after PH. Thus, we sought to formally explore the functional influence of endothelial S1P$_1$ in liver regeneration and repair. Endothelial cell (EC)-specific knockout of *S1pr1* mice were generated by breeding floxed *S1pr1* (*S1pr1*$^{f/f}$) mice with mice carrying tamoxifen-responsive Cre^{ERT2} recombinase driven by EC-specific VE-cadherin/Cdh5 promoter (Cdh5-(PAC)-Cre^{ERT2}) (27). To induce EC-specific genetic deletion of *S1pr1*,

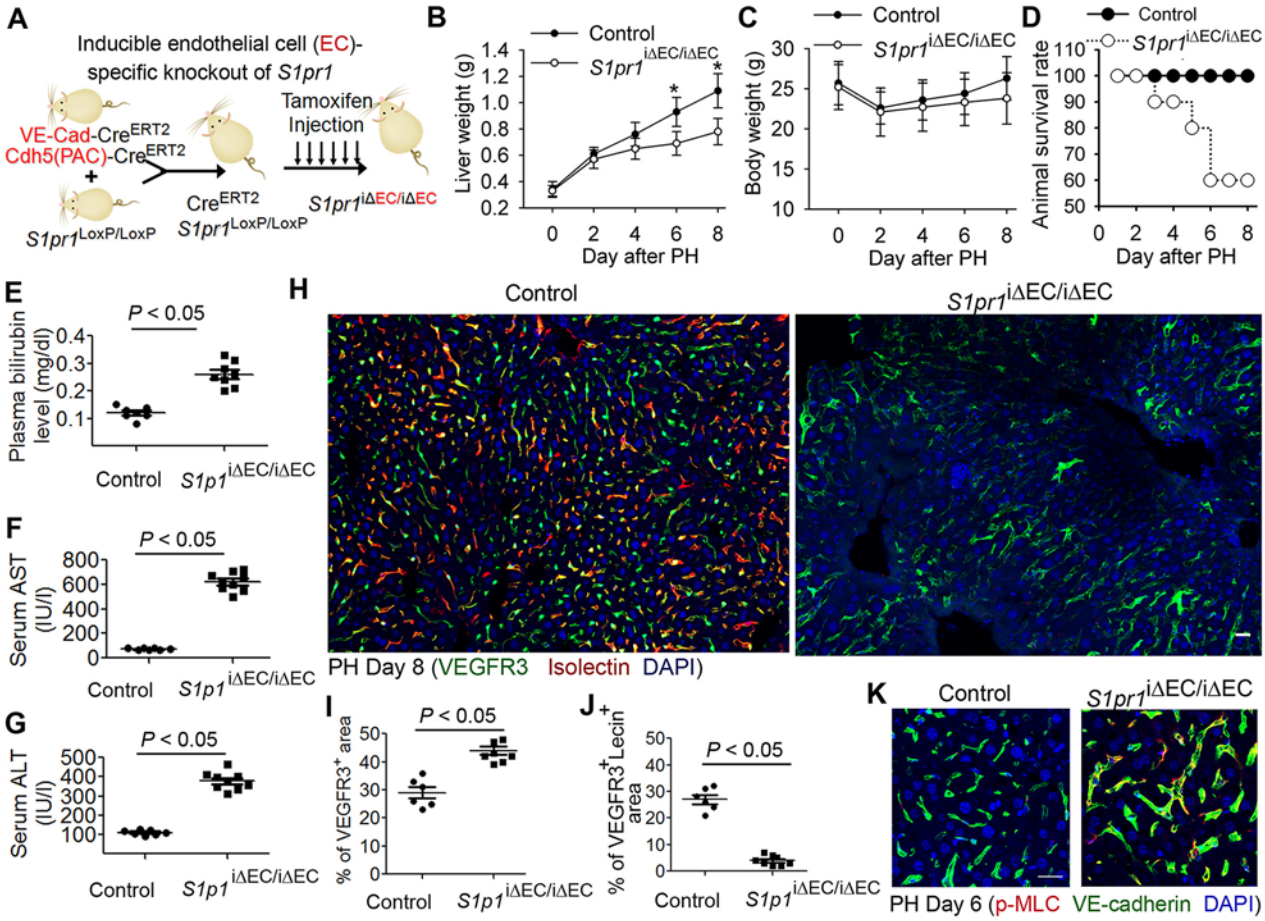

Figure 7. Liver regeneration is suppressed in mice with inducible endothelial cell-specific deletion of *S1pr1* (*S1pr1*$^{iΔEC/iΔEC}$). (**A**) Generation of inducible EC-specific deletion of *S1pr1* in adult mice. Floxed *S1pr1* (*S1pr1*$^{f/f}$) mice were bred with Cdh5-Cre^{ERT2} mice carrying tamoxifen response-Cre driven by EC-specific Cdh5/VE-cadherin promoter. Treatment of resultant mouse offspring with 200 mg/kg tamoxifen led to selective deletion of *S1pr1* in ECs (*S1pr1*$^{iΔEC/iΔEC}$). *S1pr1*$^{f/f}$ mice without Cre were similarly treated with tamoxifen and used as control group. Histology of the liver from control and *S1pr1*$^{iΔEC/iΔEC}$ mice that received sham operation is presented in Supplemental Figure 3A. (**B–D**) Recovery of liver mass (**B**), body weight (**C**) and survival rate (**D**) of hepatectomized control and *S1pr1*$^{iΔEC/iΔEC}$ mice. N= 7-8 animals per group. Statistical difference was determined by One way ANOVA throughout Figure 7. (**E–G**) Levels of plasma bilirubin and serum AST and ALT in *S1pr1*$^{iΔEC/iΔEC}$ and control mice after PH. N= 7-9 animals per group. (**H–J**) Sinusoidal vascular perfusion in *S1pr1*$^{iΔEC/iΔEC}$ and control mice after PH. Perfused vasculature was identified by examining distribution of i.v. injected B4-isolectin and VEGFR3 staining in the liver. Representative image and quantification of VEGFR3$^+$isolectin$^+$ LSECs area are shown in (**I**) and (**J**), respectively. Scale bar = 50 μm. N= 6-7 animals per group. (**K**) Rho pathway was activated in LSEC of *S1pr1*$^{iΔEC/iΔEC}$ mice after PH, as evidenced by increased level of p-MLC in VE-cadherin$^+$ LSEC. Scale bar = 50 μm.

resultant *S1pr1*$^{f/f}$Cdh5-(PAC)-Cre^{ERT2} mice were intraperitoneally treated with 200 mg/kg tamoxifen. This procedure generated mice with inducible EC-specific deletion of *S1pr1* (*S1pr1*$^{iΔEC/iΔEC}$). Tamoxifen-treated *S1pr1*$^{f/f}$Cre$^-$ mice (sex/age/weight matched littermate mice) were utilized as controls (Figure 7A).

Compared to control mice, liver mass recovery in *S1pr1*$^{iΔEC/iΔEC}$ mice was significantly attenuated, which was accompanied by higher levels of plasma bilirubin, serum AST and ALT, as well as lower survival rate after PH (Figure 7, B–G). Of note, there is negligible difference in liver morphology between control and *S1pr1*$^{iΔEC/iΔEC}$ mice (Supplemental Figure 3, A and B). Density of perfused LSEC (VEGFR3$^+$isolectin$^+$) and activation of Rho pathway were compared between hepatectomized control and *S1pr1*$^{iΔEC/iΔEC}$ mice by immunostaining (Figure 7, H–K). Moreover, livers from *S1pr1*$^{iΔEC/iΔEC}$ mice exhibited markedly higher p-MLC level in LSEC and lower number of functional LSEC than those from control mice after PH, suggesting the essential role of endothelial $S1P_1$ signaling in suppression of the Rho pathway and stimulating the regeneration of functional LSEC.

We then examined the fibrotic and thrombotic injury in *S1pr1*$^{iΔEC/iΔEC}$ mice after PH. The maladaptive remodeling of hepatic sinusoidal vasculature was observed in *S1pr1*$^{iΔEC/iΔEC}$ mice by transmission electron microscopy (Figure 8A). Immunostaining and immunoblot of fibronectin, platelet marker CD41, and fibrin β-chain further

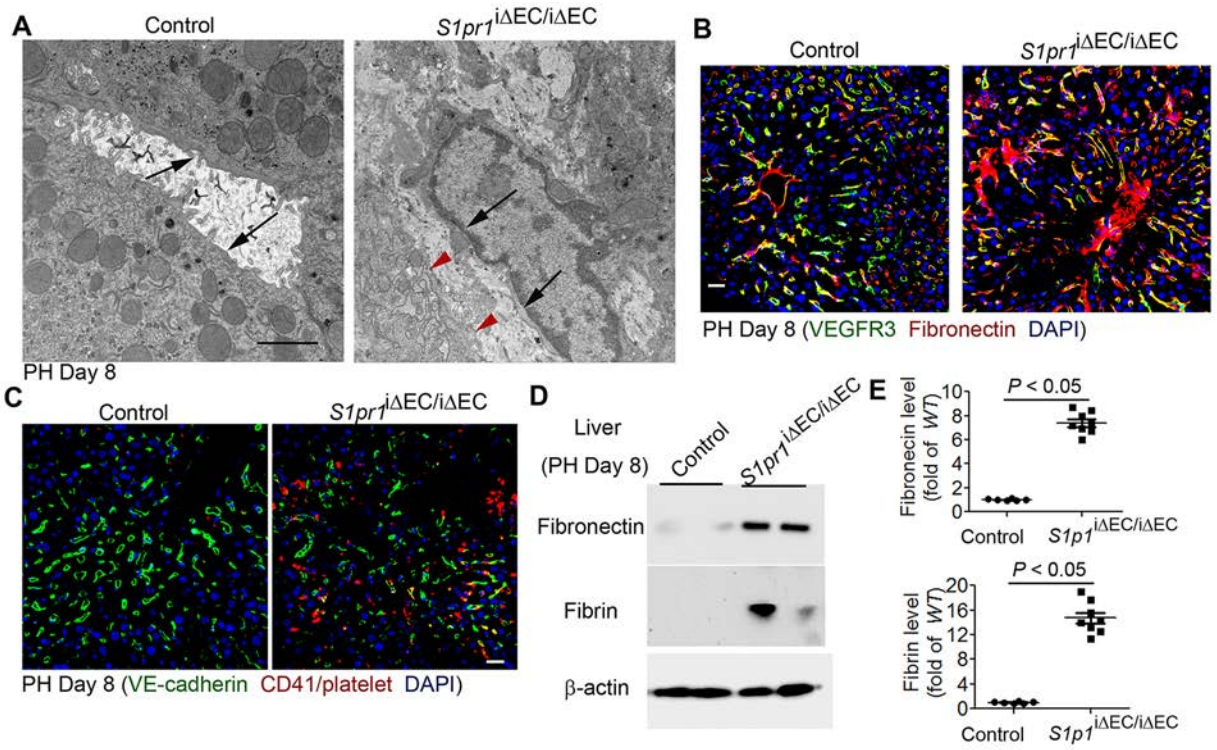

Figure 8. Development of fibrosis in hepatectomized *S1pr1*$^{i\Delta EC/i\Delta EC}$ mice. (**A** and **B**) Distribution of peri-sinusoidal matrix protein in hepatectomized *S1pr1*$^{i\Delta EC/i\Delta EC}$ and control mice. Transmission electronic microscopy was used to examine the morphology of liver sinusoids after PH (**A**), and peri-sinusoidal matrix protein expression was determined by immunostaining of both VEGFR3 and fibronectin (**B**). Scale bar = 5 μm (G), 50 μm (**B**). (**C–E**) Accumulation of platelet cells, fibrin clots, and fibronectin protein in the liver of indicated mouse groups after PH. Immunostaining of CD41 and immunoblot of fibrin and fibronectin were used to measure thrombosis and matrix deposition in the liver. Protein levels were quantified (**E**), and statistical difference was determined by One way ANOVA. Scale bar = 50 μm. N = 7-8 mice per group. Quantification of platelet distribution is shown in Supplemental Figure 3D.

demonstrated the increased peri-sinusoidal fibrosis and thrombosis in hepatectomized *S1pr1*$^{i\Delta EC/i\Delta EC}$ mice (Figure 8, B–E and Supplemental Figure 3, C and D). Therefore, hepatic sinusoidal vascular regeneration in *S1pr1*$^{i\Delta EC/i\Delta EC}$ mice recapitulates "vascular maladaptive remodeling" phenotype of *Apom*$^{-/-}$ mice after PH.

S1P$_1$ agonist administration enhanced functional hepatic mass regeneration and suppressed fibrosis in Apom$^{-/-}$ mice. The similar phenotypes observed in both *Apom*$^{-/-}$ and *S1pr1*$^{i\Delta EC/i\Delta EC}$ mice after PH suggested a direct relationship between HDL-bound S1P with endothelial S1P$_1$ signaling. Thus, we hypothesized that the defective liver regeneration seen in *Apom*$^{-/-}$ mice could be attributable to the impaired endothelial S1P$_1$ signaling caused by the absence of HDL-bound S1P. If this is true, activation of S1P$_1$ with pharmacological agonists will likely rescue the phenotype of *Apom*$^{-/-}$ mice. Indeed, administration of S1P$_1$ agonist SEW2871 enhanced the restoration of liver weight, prolonged animal survival, and augmented hepatic function recovery in *Apom*$^{-/-}$ mice after PH (Figure 9, A–C). Of importance, the regeneration of hepatic sinusoidal vasculature was also augmented by SEW2871, which was associated with decreased fibrosis and thrombosis (Figure 9, D–F, and Supplemental Figure 3E). These data suggest that ApoM$^+$HDL is epistatic to endothelial S1P$_1$ to promote liver regeneration.

Effect of S1P$_1$ agonist SEW2871 on BDL-induced fibrosis was then tested in *Apom*$^{-/-}$ mice. Oral administration of SEW2871 prevented the disruption of sinusoidal vasculature in *Apom*$^{-/-}$ mice after BDL (Figure 9G). Sinusoidal vascular perfusion was also preserved in *Apom*$^{-/-}$ mice after SEW2871 treatment (Figure 9H), implicating the pro-regenerative function of S1P$_1$ downstream of ApoM in hepatic vascular re-growth. These pharmacological and genetic "loss and gain of function" studies strongly suggest the critical contribution of endothelial S1P$_1$ to hepatic sinusoidal vascular regeneration. Loss of this essential pro-regenerative pathway leads to a dysfunctional endothelial niche, resulting in maladaptive vascular remodeling that provokes fibrosis and thrombosis in the liver (Figure 9I).

Effect of S1P$_1$ agonist SEW2871 in WT mice after cholestasis and chronic liver injury. To fully establish the translational value of endothelial S1P$_1$ signaling in hepatic repair, we tested the efficacy of SEW2871 in

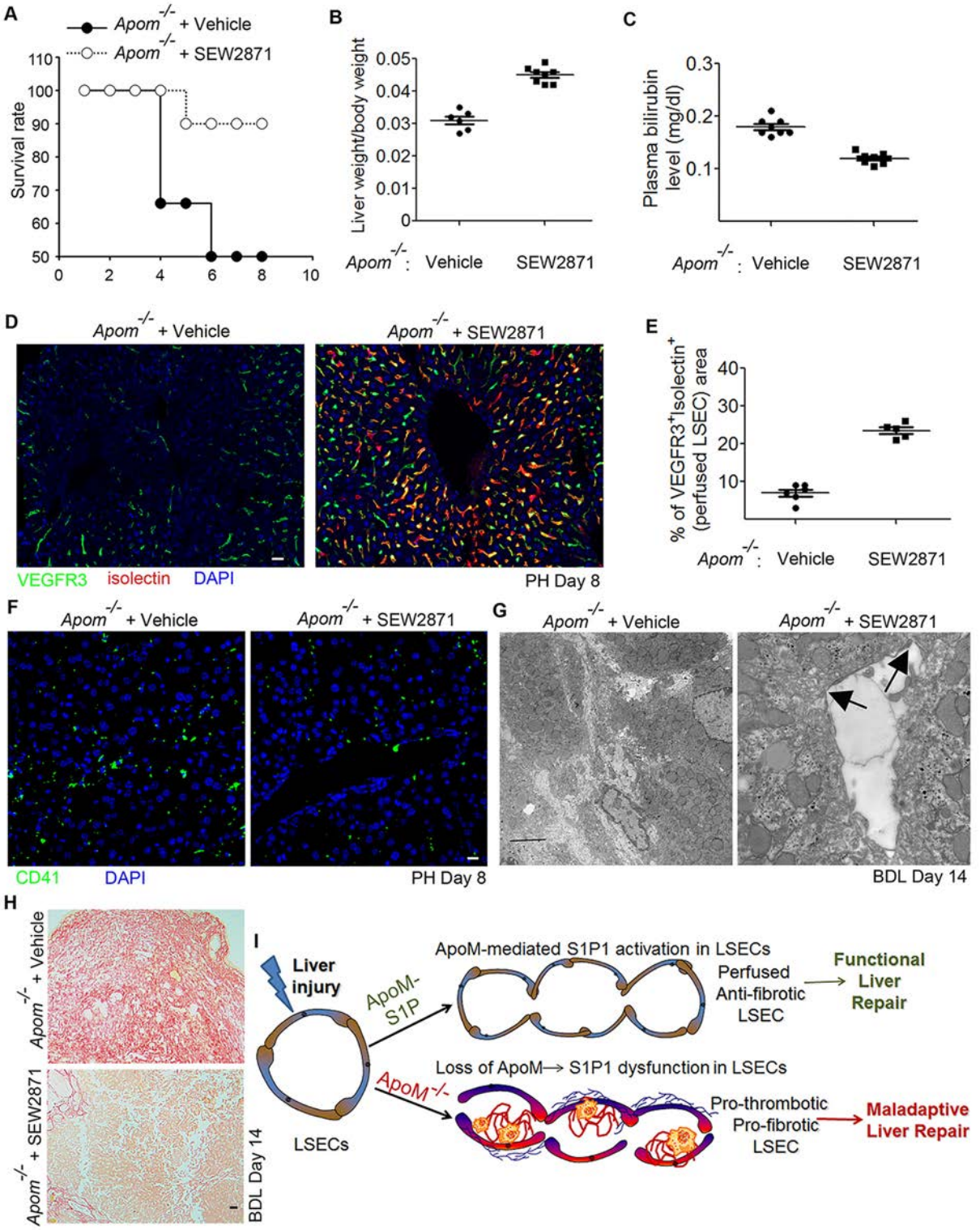

Figure 9. Effect of $S1P_1$ agonist SEW2871 on liver regeneration and fibrosis in *Apom*$^{-/-}$ mice. (**A–C**) Mouse survival rate (**A**), recovery of liver weight (**B**), and restoration of hepatic function (**C**) were tested in *Apom*$^{-/-}$ mice after oral gavage of $S1P_1$ agonist SEW2871 or vehicle after PH. Plasma bilirubin level was measured to examine the functional recovery of liver mass. N = 6-8 mice per group. 10 mg/kg/day SEW2871 was administered via oral gavage for seven days immediately after BDL and another seven days between day 14 and day 21. $P < 0.05$ between vehicle and SEW2871 treated groups in B and C. Statistical difference was determined by One way ANOVA. (**D–F**) Sinusoidal vascular structure and platelet cell deposition in hepatectomized *ApoM*$^{-/-}$ mice treated with SEW2871. Vascular perfusion and platelet distribution in the liver were determined by staining of LSEC marker VEGFR3, i.v. injected B4-isolectin (**D** and **E**), and platelet marker CD41 (**F**). Immunostaining image is shown in (**D**), and perfused LSEC number was measured by quantification of VEGFR3$^+$Isolectin$^+$ area percentage (**E**). SEW2871 improved the perfusion of VEGFR3$^+$ LSEC in *Apom*$^{-/-}$ mice. Note that $S1P_1$ agonist treatment also reduced platelet cell number in the liver of *Apom*$^{-/-}$ mice (Supplemental Figure 3E), suggesting the alleviated thrombosis. N = 5 mice per group. Scale bar = 50 μm.

(**G** and **H**) SEW2871 reduced maladaptive vascular remodeling and associated fibrosis in *Apom*$^{-/-}$ mouse liver after BDL. Vascular morphology alteration in treated *Apom*$^{-/-}$ mice was assessed by electron microscopy (**G**), and collagen deposition was measured by Sirius red staining (**H**). BDL disrupted the sinusoidal vasculature structure in *Apom*$^{-/-}$ mice, and SEW2871 attenuated this maladaptive vascular remodeling, resulting in a sinusoidal structure displaying unperturbed cell junction (arrow) and endothelial morphology. Scale bar = 5 μm (G), 50 μm (**H**). (**I**) HDL-bound S1P and pharmacological agonist specific for $S1P_1$ modulates liver regeneration. Perturbation of this pro-regenerative endothelial $S1P_1$ pathway prohibits sinusoidal vascular regeneration and evokes a maladaptive vascular remodeling instigating fibrosis and thrombosis.

normal *WT* mice in BDL model. Treatment of *WT* mice with SEW2871 promoted activation of endothelial $S1P_1$ activation (GFP expression in $S1P_1$-GFP mice) (Figure 10A) and attenuated Rho activation in LSEC as determined by p-MLC staining (Figure 10B). SEW2871 also prevented hepatic parenchymal damage after BDL, as demonstrated by lower levels of serum ALT, AST and bilirubin than vehicle treated mice (Figure 10C). Consequently, both thrombosis and fibrosis in the damaged liver were alleviated by administration of SEW2871 after BDL (Figure 10, D and F).

The anti-fibrotic effect of SEW2871 was subsequently assessed in a repeated liver injury model. Hepatotoxin carbon tetrachloride (CCl_4) was intraperitoneally (i.p.) administered to *WT* mice for ten times to induce chronic liver injury (Figure 11A). Fibrosis and vascular perfusion were compared between SEW2871 and vehicle-treated animals. SEW2871 improved hepatic vascular perfusion and reduced SMA protein level in the CCl_4-injured livers (Figure 11, B and C). Improved vascular function by SEW2871 was associated with reduced liver fibrosis (Figure 11, D and E). As such, administered SEW2871 activates $S1P_1$ signaling in LSEC after liver injury, enhances regeneration of sinusoidal vasculature, and ameliorates hepatic damage and associated fibrosis.

Discussion

Regeneration of the liver requires formation of perfused vascular system. Our study demonstrates that activation of the endothelial $S1P_1$ receptor by either its natural ligand (HDL-bound S1P) or pharmacological agonist SEW2871 promotes hepatic regeneration and attenuates fibrosis. The contribution of HDL constituent ApoM in this process underscores the delicate control of sinusoidal vessel assembly by $S1P_1$ in liver regeneration. HDL-bound S1P was recently shown to act as a biased agonist of endothelial $S1P_1$ to initiate β-arrestin-dependent anti-inflammatory responses (53). In the current study, we provide evidence that $ApoM^+$HDL stimulates the formation of new sinusoidal vessel after PH and BDL, and endothelial $S1P_1$ is needed for the circulating HDL-bound S1P to drive the assembly of nascent LSECs into metabolically functional vasculature.

Here we show that lipoprotein HDL regulates the formation of perfused and metabolically functional LSECs. Endothelial $S1P_1$ responds to the circulating HDL-bound S1P to drive the formation and remodeling of functional LSECs. Requirement of both HDL and S1P in this process underscores the complex control of sinusoidal vessel assembly in liver regeneration. Considering that liver is the major metabolic organ that synthesizes HDL, it is likely that HDL produced by expanding hepatocytes stimulates regeneration via activation of $S1P_1$ on sinusoidal vessels (63, 64). This finding might advance our understanding of hepatocyte-LSEC signaling crosstalk (24, 25, 65) that promotes regeneration and prevents fibrosis, and targeting of maladapted vascular system might spur regeneration and prevent fibrosis (31, 66–69).

There might be multi-step feed-forward loops involved in the drastically exacerbated fibrosis in *Apom* knockout mice after injury. First, immediately after BDL, lack of *Apom* in mice (absence of HDL-bound S1P) causes more severe vascular dysfunction and occlusion in the damaged liver (due to impaired endothelial $S1P_1$ signaling). Then, this vascular dysfunction exacerbates the existent cholestic liver injury by triggering more vascular damage, including fibrin clot formation, vascular occlusion, and deposition of perivascular matrix protein. Subsequently, increased vascular stress reinforces the existent liver injury to impose more damage to the liver, increasing fibrosis progression rate. As a result, enhanced fibrosis in the damaged *Apom*$^{-/-}$ liver markedly disrupts vascular perfusion. The improved hepatic repair in injured *Apom* knockout mice by $S1P_1$ agonist SEW2871 also helped to establish the epistatic relationships between ApoM and $S1P_1$ signaling in liver regeneration.

Here we have found that $S1P_1$ agonist SEW2871 reduces liver damage and fibrosis in both cholestasis and chronic hepatotoxin-mediated injury models. SEW2871 also restores the defective liver regeneration in mice lacking ApoM after PH. The beneficial effect of SEW2871 in all these tested liver repair models suggests that S1P1 signaling is largely connected to limiting liver damage regardless of etiology. Thus,

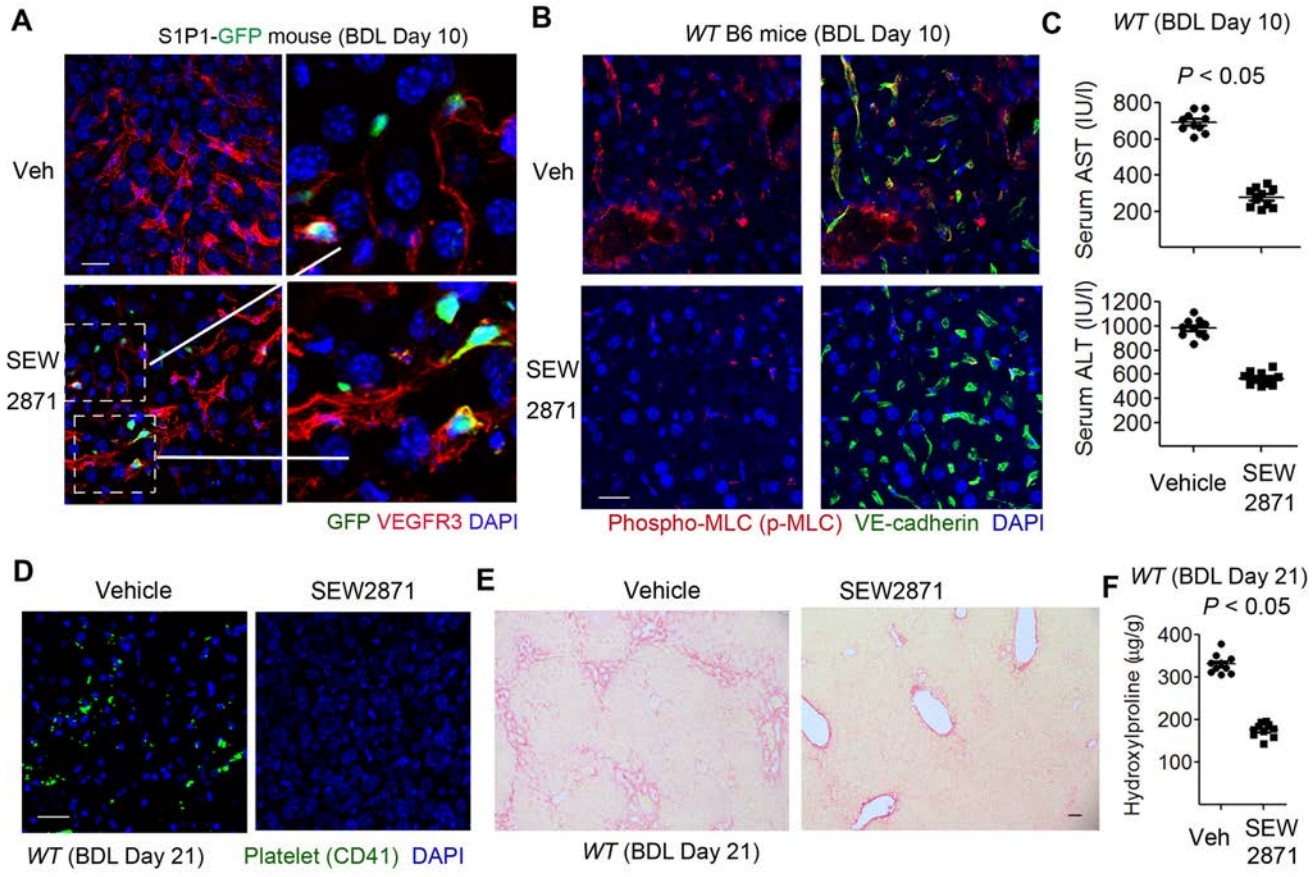

Figure 10. SEW2871 promotes liver repair in *WT* mice after BDL injury. (**A**) Activation of $S1P_1$ signaling by SEW2871 in mouse LSEC after BDL. S1P1-GFP mice were treated with SEW2871 and subjected to BDL, GFP was co-stained with LSEC marker VEGFR3. Scale bar = 50 μm. (**B–F**) SEW2871 reduced Rho activation in LSEC (**B**), prevented liver damage (**C**), decreased thrombosis (**D**) and fibrosis (**E** and **F**) in *WT* mice following BDL. Rho activation was tested by staining of p-MLC, thrombosis was assessed by immunostaining of CD41, and liver fibrosis was determined by sirius red staining and measurement of hydroxyproline level; Scale bar = 50 μm. N = 11 mice per group in panel **C** and **F**, and statistical difference was determined by One way ANOVA.

triggering this important hepatogenic ApoM-endothelial $S1P_1$ pathway might provide effective therapeutic avenues for fibrosis-related hepatic diseases. In contrast to other S1P receptor-targeted compounds that suppress immune cell trafficking by functional antagonism of lymphocyte $S1P_1$ receptor, SEW2871 is a much less potent as a functional antagonist (70). In the future, this finding can be extended by testing new generations of biased $S1P_1$ agonist in broader scenario of liver repair.

Whether HDL-S1P affects S1P receptors on other liver cell types such as stellate cells (1, 2, 18, 20) are not known at present. In this context, it was shown that signaling via $S1P_2$ and $S1P_3$ receptors in these cells may drive fibrogenic responses (71). These two receptor subtypes are coupled to distinct downstream signaling effectors and therefore drive the expression of pro-fibrogenic genes such as *Ctgf* via the Hippo/Yap signaling pathway (72, 73).

Thus, the generation of S1P and its chaperones in the liver, together with signaling by HDL-bound S1P on S1P receptors expressed in various liver cell types constitutes a finely balanced signaling system involved in maintaining metabolic homeostasis, inducing regeneration, as well as preventing pathological remodeling events (63, 74). Ligand-based pro-regenerative property of endothelial $S1P_1$ is pharmacologically tractable and could help to design novel treatments for fibrosis-related liver disorders.

Methods

Endothelial cell (EC)-specific gene deletion strategy. C57BL/6J mice were obtained from Jackson Laboratories. *S1pr1*$^{f/f}$ mice were previously described (54) and crossed with Cdh5-(PAC)-Cre^{ERT2} mice (27) to establish the Cre^{+}*S1pr1*$^{f/f}$ mice and control *S1pr1*$^{f/f}$ mice. To induce endothelial cell-specific knockdown of *S1p1*, generated *Cre*$^{+}$*S1pr1*$^{f/f}$ mice and control *S1pr1*$^{f/f}$ mice were treated with tamoxifen. Briefly, 6-week-old male and

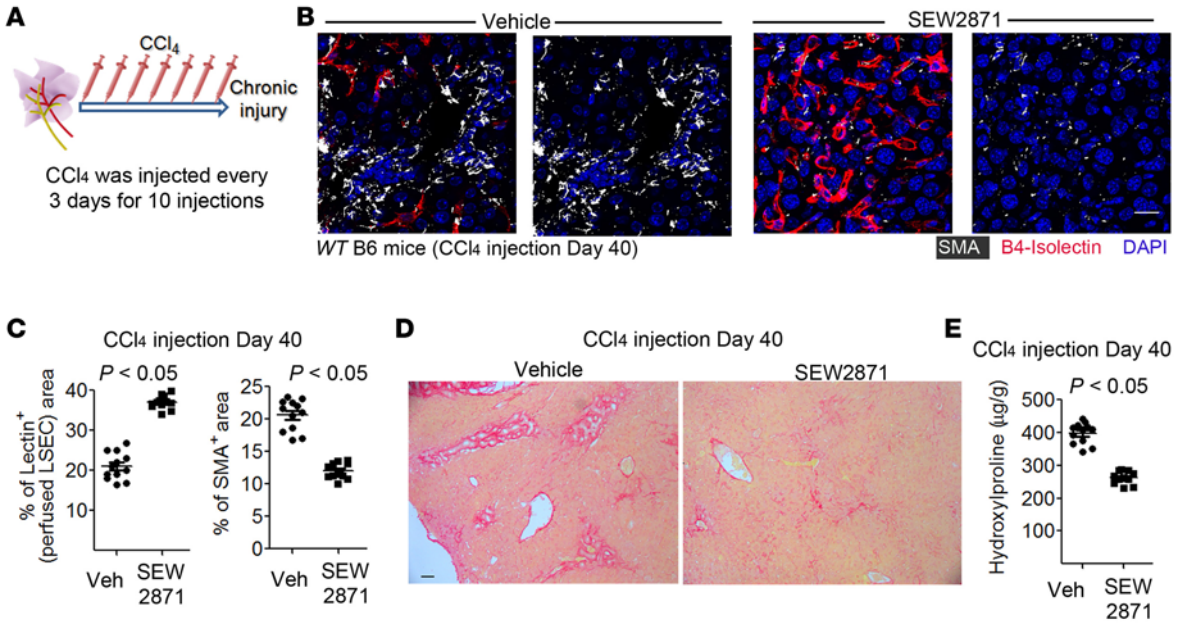

Figure 11. SEW2871 decreases liver fibrosis in *WT* mice after repetitive injection of carbon tetrachloride (CCl_4). (**A**) Chronic liver injury was induced in mice by injection of CCl_4 every three days for 10 injections. Mice were sacrificed at day 40 after first injection. SEW2871 was given to mice after third injection. (**B–E**) SEW2871 restored vascular perfusion and prevented liver fibrosis after repeated CCl_4 injection. Vascular perfusion was tested by visualization of i.v. injected B4-isolectin (**B** and **C**), and fibrosis was determined by measuring levels of SMA (**B** and **C**), Collagen (**D**), and hydroxyproline (**E**) in the injured liver. Veh, vehicle. Scale bar = 50 μm. N = 11 mice per group in panel **C** and **E**, and statistical difference was calculated by One way ANOVA.

female mice were treated with tamoxifen intraperitoneally at a dose of 200 mg kg^{-1} in sunflower oil for 6 days, and interrupted for 3 days after the third dose. After 3 days of rest, the fourth dose was injected for an additional 3 days. After three weeks of tamoxifen treatment, deletion of target genes in ECs was corroborated by quantitative PCR, and mice were used for PH, BDL, and CCl_4 treatment.

Mouse liver regeneration model. Mouse PH model was used to induce liver regeneration (24). Mice were anaesthetized by 100 mg/kg intraperitoneal ketamine and 10 mg/kg xylazine. Midline laparotomy was performed in the anaesthetized mice, and three most anterior lobes (right medial, left medial and left lateral lobes) containing 70% of the liver weight were surgically removed. Briefly, after opening the upper abdomen and the exposure of the liver, the left lobe to be removed was lifted. A 5-0 silk suture tie (Roboz) was placed under the lobe and positioned to the origin of the lobe. After three knots were tied, the tied lobe distal to the suture was resected by a microdissecting scissor. This surgical procedure was then repeated for the other median lobes to complete PH procedure. Following surgical removal of 70% of liver mass, the peritoneum was re-approximated, and the skin was closed. Sham-operated mice underwent laparotomy without lobe resection.

Regeneration of liver mass and function was assessed by measuring the weight of residual liver lobes and mouse body weight and levels of plasma bilirubin, serum AST and ALT at indicated time points after PH.

Liver injury and fibrosis models. Six to eight-week-old mice were subjected to bile duct ligation to induce mouse cirrhotic liver injury model (31). To perform BDL, mice were subjected to a mid-abdominal incision, under general anesthesia. The common bile duct was ligated in two adjacent positions approximately 1 cm from the porta hepatis. The duct was then severed by incision between the two sites of ligation. Repeated injections of CCl_4 were used to induce chronic liver injury (31). CCl_4 was diluted in oil to yield a concentration of 40% (0.64 mg ml^{-1}) and injected to mice every three days at a dose of 1.6 mg/kg. Mice were sacrificed 10 days after the 10th CCl_4 injection, and the livers were harvested for analysis of morphology and fibrosis.

To selectively induce $S1P_1$ activation, 10 mg/kg/day SEW2871 was administered via oral gavage. Stock solution of SEW2871 was dissolved in 10% DMSO/25% Tween 20 (v/v). This solvent was used as vehicle for comparison. 10 mg/kg/day SEW2871 was administered to both *Apom* knockout and *WT* mice via oral gavage for seven days immediately after BDL and another seven days between day 14 and day 21. 10 mg/kg SEW2871 was also administered into *WT* mice after third injection of CCl_4 and

every two days thereafter till last injection. At indicated days, mice were killed and whole liver tissues were harvested for fibrosis analysis. Collagen I deposition was tested by Sirius red staining, and SMA (5 μg/ml, Abcam, CA, catalogue number ab5694), fibronectin (5 μg/ml, Abcam, CA, catalogue number ab2413) protein levels were measured by immunoblot. Fibrin β-chain was detected by monoclonal antibody Clone 350 from American Diagnostica (5 μg/ml), which recognizes fibrin neotope on beta-chain.

Measurement of fibrosis. Liver fibrosis was assessed after CCl_4 injection and BDL. Collagen deposition was determined by Sirius red staining, and hepatic hydroxyproline level was measured (31, 66). Liver lobes were weighed, homogenized, and baked in 12 N hydrochloric acid. Obtained samples were added to 1.4% chloramine T in 0.5 M sodium acetate/10% isopropanol (Sigma) and then incubated with Erlich's solution at 65 °C. Absorbance at 540 nm wavelength was measured and comparing to hydroxyproline standard curve, Content of hydroxyproline in tissue lysate was quantified based on the liver weight. Sirius red staining on liver section was carried out, following the protocol of Lilai Biology (Chengdu, China) and Histoserv (Germantown, MD) (24, 65, 75, 76).

Immunostaining and histological analysis of liver cryosections. Liver tissues were harvested for histological analysis (24, 31). Mouse tissues were fixed with 4% PFA and cryopreserved in OCT. For immunofluorescent (IF) microscopy, the liver sections (10 μm) were blocked (5% donkey serum/0.3% Triton X-100) and incubated in primary Abs: anti-CD41 (mAb, 5 μg/ml, BD Biosciences, CA, Clone MWReg30), anti-VE-cadherin polyclonal Ab (10 μg/ml, R&D Systems, MN, Catalogue number: AF1002), anti-VEGFR3 (mAb, 5 μg/ml, Imclone, NY, Clone mF4-31C1), anti-fibronectin (5 μg/ml, Abcam, CA, Catalogue number: ab2413), anti-SMA (5 μg/ml, Abcam, CA, Catalogue number: ab5694), and anti-pMLC (5 μg/ml, Cell Signaling, Catalogue number: 3674S). After incubation in fluorophore-conjugated secondary antibodies (2.5 μg/ml, Jackson ImmunoResearch, PA), sections were counterstained with DAPI (Invitrogen, CA).

Image acquisition and analysis. Histology analysis and Sirius red staining of liver slides were captured with Olympus BX51 microscope (Olympus America, NY), and fluorescent images were recorded on AxioVert LSM710 confocal microscope (Zeiss). Co-staining of VE-cadherin with SMA and desmin was carried out. Digital images were analyzed using Image J (NIH, MD). Investigators that performed mouse liver regeneration and repair experiments and who determined the extent and pattern of cell proliferation and activation were randomly assigned with animal samples from different experimental groups and were blinded to the genotype of samples.

Statistics. All data were presented as the mean ± standard error of mean (S.E.M). Comparisons between different groups were made using One way ANOVA. Statistical significance was set at $P<0.05$.

Study Approval. All animal experiments were performed under the guidelines set by the Institutional Animal Care and Use Committee at Weill Cornell Medicine, New York, and Sichuan University, Chengdu, China.

Author Contributions

BSD designed the study, performed the experiments, interpreted the results, and wrote the paper. KL, YS, YC, SLS, BJ, DC, and ZC performed the experiments and analyzed the data. CC, LB, SRS, SR analyzed the data. TH designed the experiments and edited the manuscript.

Acknowledgments

TH is supported by National Heart, Lung, and Blood Institute (R01HL089934 and R37 HL067330). This work was also supported by the Ansary Stem Cell Institute, National Scientist Development Grant from the American Heart Association (12SDG1213004), National Heart, Lung, and Blood Institute (R01HL130826), and Key National Research and Development Program focused on Stem Cell and Translational Research (2016YFA0101600) from Ministry of Science and Technology, China. SR is supported by the Empire State Stem Cell Board and New York State Department of Health grants (C024180, C026438, C026878, C028117), National Heart, Lung, and Blood Institute (R01HL097797 and R01HL119872). CC is supported by NNF13OC0003898 - Novonordisk foundation, excellence project. SRS is supported by National Institute of Health (R01AI085166).

Address correspondence to: Bi-Sen Ding, Keyuan 4th Avenue, Chengdu, 610041, China. Phone: 86.28.85595546; E-mail: bid2004@med.cornell.edu or dingbisen@scu.edu.cn.

1. Friedman SL, Sheppard D, Duffield JS, Violette S. Therapy for fibrotic diseases: nearing the starting line. *Sci Transl Med*. 2013;5(167):167sr1.
2. Seki E, et al. TLR4 enhances TGF-beta signaling and hepatic fibrosis. *Nat Med*. 2007;13(11):1324–1332.
3. Huebert RC, et al. Aquaporin-1 facilitates angiogenic invasion in the pathological neovasculature that accompanies cirrhosis. *Hepatology*. 2010;52(1):238–248.
4. Apte U, et al. Activation of Wnt/beta-catenin pathway during hepatocyte growth factor-induced hepatomegaly in mice. *Hepatology*. 2006;44(4):992–1002.
5. Nishikawa T, et al. Resetting the transcription factor network reverses terminal chronic hepatic failure. *J Clin Invest*. 2015;125(4):1533–1544.
6. Boulter L, et al. Macrophage-derived Wnt opposes Notch signaling to specify hepatic progenitor cell fate in chronic liver disease. *Nat Med*. 2012;18(4):572–579.
7. Diehl AM, Chute J. Underlying potential: cellular and molecular determinants of adult liver repair. *J Clin Invest*. 2013;123(5):1858–1860.
8. Huang W, et al. Nuclear receptor-dependent bile acid signaling is required for normal liver regeneration. *Science*. 2006;312(5771):233–236.
9. Mahley RW. Apolipoprotein E: cholesterol transport protein with expanding role in cell biology. *Science*. 1988;240(4852):622–630.
10. Zaret KS, Grompe M. Generation and regeneration of cells of the liver and pancreas. *Science*. 2008;322(5907):1490–1494.
11. Monga SP, Monga HK, Tan X, Mulé K, Pediaditakis P, Michalopoulos GK. Beta-catenin antisense studies in embryonic liver cultures: role in proliferation, apoptosis, and lineage specification. *Gastroenterology*. 2003;124(1):202–216.
12. Yanger K, et al. Adult hepatocytes are generated by self-duplication rather than stem cell differentiation. *Cell Stem Cell*. 2014;15(3):340–349.
13. Lesurtel M, et al. Platelet-derived serotonin mediates liver regeneration. *Science*. 2006;312(5770):104–107.
14. Matsuo T, Yamaguchi S, Mitsui S, Emi A, Shimoda F, Okamura H. Control mechanism of the circadian clock for timing of cell division in vivo. *Science*. 2003;302(5643):255–259.
15. Fausto N, Campbell JS, Riehle KJ. Liver regeneration. *Hepatology*. 2006;43(2 Suppl 1):S45–S53.
16. Michalopoulos GK, DeFrances MC. Liver regeneration. *Science*. 1997;276(5309):60–66.
17. Huh CG, Factor VM, Sánchez A, Uchida K, Conner EA, Thorgeirsson SS. Hepatocyte growth factor/c-met signaling pathway is required for efficient liver regeneration and repair. *Proc Natl Acad Sci U S A*. 2004;101(13):4477–4482.
18. Yin C, Evason KJ, Asahina K, Stainier DY. Hepatic stellate cells in liver development, regeneration, and cancer. *J Clin Invest*. 2013;123(5):1902–1910.
19. Diehl AM. Neighborhood watch orchestrates liver regeneration. *Nat Med*. 2012;18(4):497–499.
20. Passino MA, Adams RA, Sikorski SL, Akassoglou K. Regulation of hepatic stellate cell differentiation by the neurotrophin receptor p75NTR. *Science*. 2007;315(5820):1853–1856.
21. Matsumoto K, Yoshitomi H, Rossant J, Zaret KS. Liver organogenesis promoted by endothelial cells prior to vascular function. *Science*. 2001;294(5542):559–563.
22. Wang L, Wang X, Xie G, Wang L, Hill CK, DeLeve LD. Liver sinusoidal endothelial cell progenitor cells promote liver regeneration in rats. *J Clin Invest*. 2012;122(4):1567–1573.
23. Wang B, Zhao L, Fish M, Logan CY, Nusse R. Self-renewing diploid Axin2(+) cells fuel homeostatic renewal of the liver. *Nature*. 2015;524(7564):180–185.
24. Ding BS, et al. Inductive angiocrine signals from sinusoidal endothelium are required for liver regeneration. *Nature*. 2010;468(7321):310–315.
25. Hu J, et al. Endothelial cell-derived angiopoietin-2 controls liver regeneration as a spatiotemporal rheostat. *Science*. 2014;343(6169):416–419.
26. LeCouter J, et al. Angiogenesis-independent endothelial protection of liver: role of VEGFR-1. *Science*. 2003;299(5608):890–893.
27. Wang Y, et al. Ephrin-B2 controls VEGF-induced angiogenesis and lymphangiogenesis. *Nature*. 2010;465(7297):483–486.
28. Wynn TA, Ramalingam TR. Mechanisms of fibrosis: therapeutic translation for fibrotic disease. *Nat Med*. 2012;18(7):1028–1040.
29. Wynn TA, Chawla A, Pollard JW. Macrophage biology in development, homeostasis and disease. *Nature*. 2013;496(7446):445–455.
30. Straub AC, et al. Arsenic-stimulated liver sinusoidal capillarization in mice requires NADPH oxidase-generated superoxide. *J Clin Invest*. 2008;118(12):3980–3989.
31. Ding BS, et al. Divergent angiocrine signals from vascular niche balance liver regeneration and fibrosis. *Nature*. 2014;505(7481):97–102.
32. Simonetto DA, et al. Chronic passive venous congestion drives hepatic fibrogenesis via sinusoidal thrombosis and mechanical forces. *Hepatology*. 2015;61(2):648–659.
33. Liu L, et al. The microenvironment in hepatocyte regeneration and function in rats with advanced cirrhosis. *Hepatology*. 2012;55(5):1529–1539.
34. Ackah E, et al. Akt1/protein kinase Balpha is critical for ischemic and VEGF-mediated angiogenesis. *J Clin Invest*. 2005;115(8):2119–2127.
35. Zeisberg EM, et al. Endothelial-to-mesenchymal transition contributes to cardiac fibrosis. *Nat Med*. 2007;13(8):952–961.
36. Thannickal VJ, Zhou Y, Gaggar A, Duncan SR. Fibrosis: ultimate and proximate causes. *J Clin Invest*. 2014;124(11):4673–4677.
37. Duffield JS, Lupher M, Thannickal VJ, Wynn TA. Host responses in tissue repair and fibrosis. *Annu Rev Pathol*. 2013;8:241–276.
38. Mehal WZ, Iredale J, Friedman SL. Scraping fibrosis: expressway to the core of fibrosis. *Nat Med*. 2011;17(5):552–553.
39. Marin EP, Derakhshan B, Lam TT, Davalos A, Sessa WC. Endothelial cell palmitoylproteomic identifies novel lipid-modified targets and potential substrates for protein acyl transferases. *Circ Res*. 2012;110(10):1336–1344.
40. Skuli N, et al. Endothelial HIF-2α regulates murine pathological angiogenesis and revascularization processes. *J Clin Invest*. 2012;122(4):1427–1443.
41. Sun K, Tordjman J, Clément K, Scherer PE. Fibrosis and adipose tissue dysfunction. *Cell Metab*. 2013;18(4):470–477.
42. Cao Y. Angiogenesis and vascular functions in modulation of obesity, adipose metabolism, and insulin sensitivity. *Cell Metab*. 2013;18(4):478–489.

43. Aragonés J, Fraisl P, Baes M, Carmeliet P. Oxygen sensors at the crossroad of metabolism. *Cell Metab*. 2009;9(1):11–22.
44. Arany Z, et al. HIF-independent regulation of VEGF and angiogenesis by the transcriptional coactivator PGC-1alpha. *Nature*. 2008;451(7181):1008–1012.
45. Rautou PE, et al. Hepatocyte tissue factor contributes to the hypercoagulable state in a mouse model of chronic liver injury. *J Hepatol*. 2016;64(1):53–59.
46. Antoniak S, et al. PAR-1 contributes to the innate immune response during viral infection. *J Clin Invest*. 2013;123(3):1310–1322.
47. Lee S, et al. Autocrine VEGF signaling is required for vascular homeostasis. *Cell*. 2007;130(4):691–703.
48. Aspinall AI, et al. CX(3)CR1 and vascular adhesion protein-1-dependent recruitment of CD16(+) monocytes across human liver sinusoidal endothelium. *Hepatology*. 2010;51(6):2030–2039.
49. Lee JS, Semela D, Iredale J, Shah VH. Sinusoidal remodeling and angiogenesis: a new function for the liver-specific pericyte? *Hepatology*. 2007;45(3):817–825.
50. Sawitza I, Kordes C, Reister S, Häussinger D. The niche of stellate cells within rat liver. *Hepatology*. 2009;50(5):1617–1624.
51. Blaho VA, et al. HDL-bound sphingosine-1-phosphate restrains lymphopoiesis and neuroinflammation. *Nature*. 2015;523(7560):342–346.
52. Christoffersen C, et al. Endothelium-protective sphingosine-1-phosphate provided by HDL-associated apolipoprotein M. *Proc Natl Acad Sci U S A*. 2011;108(23):9613–9618.
53. Galvani S, et al. HDL-bound sphingosine 1-phosphate acts as a biased agonist for the endothelial cell receptor S1P1 to limit vascular inflammation. *Sci Signal*. 2015;8(389):ra79.
54. Jung B, et al. Flow-regulated endothelial S1P receptor-1 signaling sustains vascular development. *Dev Cell*. 2012;23(3):600–610.
55. Gaengel K, et al. The sphingosine-1-phosphate receptor S1PR1 restricts sprouting angiogenesis by regulating the interplay between VE-cadherin and VEGFR2. *Dev Cell*. 2012;23(3):587–599.
56. Deng J, et al. S1PR1-STAT3 signaling is crucial for myeloid cell colonization at future metastatic sites. *Cancer Cell*. 2012;21(5):642–654.
57. Smyth SS, Cheng HY, Miriyala S, Panchatcharam M, Morris AJ. Roles of lysophosphatidic acid in cardiovascular physiology and disease. *Biochim Biophys Acta*. 2008;1781(9):563–570.
58. Tager AM, et al. The lysophosphatidic acid receptor LPA1 links pulmonary fibrosis to lung injury by mediating fibroblast recruitment and vascular leak. *Nat Med*. 2008;14(1):45–54.
59. Kono M, Tucker AE, Tran J, Bergner JB, Turner EM, Proia RL. Sphingosine-1-phosphate receptor 1 reporter mice reveal receptor activation sites in vivo. *J Clin Invest*. 2014;124(5):2076–2086.
60. Lee MJ, et al. Akt-mediated phosphorylation of the G protein-coupled receptor EDG-1 is required for endothelial cell chemotaxis. *Mol Cell*. 2001;8(3):693–704.
61. Vouret-Craviari V, Bourcier C, Boulter E, van Obberghen-Schilling E. Distinct signals via Rho GTPases and Src drive shape changes by thrombin and sphingosine-1-phosphate in endothelial cells. *J Cell Sci*. 2002;115(Pt 12):2475–2484.
62. Zhou Z, et al. Cerebral cavernous malformations arise from endothelial gain of MEKK3-KLF2/4 signalling. *Nature*. 2016;532(7597):122–126.
63. Jin W, et al. Hepatic proprotein convertases modulate HDL metabolism. *Cell Metab*. 2007;6(2):129–136.
64. Tatematsu S, et al. Endothelial lipase is a critical determinant of high-density lipoprotein-stimulated sphingosine 1-phosphate-dependent signaling in vascular endothelium. *Arterioscler Thromb Vasc Biol*. 2013;33(8):1788–1794.
65. Rafii S, et al. Platelet-derived SDF-1 primes the pulmonary capillary vascular niche to drive lung alveolar regeneration. *Nat Cell Biol*. 2015;17(2):123–136.
66. Cao Z, et al. Targeting of the pulmonary capillary vascular niche promotes lung alveolar repair and ameliorates fibrosis. *Nat Med*. 2016;22(2):154–162.
67. Carmeliet P, Jain RK. Molecular mechanisms and clinical applications of angiogenesis. *Nature*. 2011;473(7347):298–307.
68. Bogdanovich S, et al. Human IgG1 antibodies suppress angiogenesis in a target-independent manner. *Signal Transduct Target Ther*. 2016;1.
69. Yasuma R, et al. Intravenous immune globulin suppresses angiogenesis in mice and humans. *Signal Transduct Target Ther*. 2016;1.
70. Jo E, et al. S1P1-selective in vivo-active agonists from high-throughput screening: off-the-shelf chemical probes of receptor interactions, signaling, and fate. *Chem Biol*. 2005;12(6):703–715.
71. Kageyama Y, et al. Antagonism of sphingosine 1-phosphate receptor 2 causes a selective reduction of portal vein pressure in bile duct-ligated rodents. *Hepatology*. 2012;56(4):1427–1438.
72. Yu FX, et al. Regulation of the Hippo-YAP pathway by G-protein-coupled receptor signaling. *Cell*. 2012;150(4):780–791.
73. Yimlamai D, et al. Hippo pathway activity influences liver cell fate. *Cell*. 2014;157(6):1324–1338.
74. Owens AP, et al. Monocyte tissue factor-dependent activation of coagulation in hypercholesterolemic mice and monkeys is inhibited by simvastatin. *J Clin Invest*. 2012;122(2):558–568.
75. Cao Z, et al. Angiocrine factors deployed by tumor vascular niche induce B cell lymphoma invasiveness and chemoresistance. *Cancer Cell*. 2014;25(3):350–365.
76. Ding BS, et al. Endothelial-derived angiocrine signals induce and sustain regenerative lung alveolarization. *Cell*. 2011;147(3):539–553.